

Evaluation of Virtual Fixtures for Robot-Assisted Cochlear Implant Insertion

Paul Wilkening, *Member, IEEE*, Wade Chien, MD, Berk Gonenc, *Student Member, IEEE*, John Niparko, MD, Jin U. Kang, *Member, IEEE*, Iulian Iordachita, *Senior Member, IEEE*, and Russell H. Taylor, *Fellow, IEEE*

Abstract— Cochlear implantation requires the placement of an electrode array into the cochlea of patients with severe to profound hearing loss. As the array is placed without direct visualization, robotic guidance has significant potential to improve upon the precision of electrode placement within the cochlea. Here, we evaluate the repeatability of robot-assisted placement of an implant array to an optimal deployment point within a phantom cochlea. This system guides the insertion of the implant by enacting virtual fixtures. When compared to the standard manual method of insertion, we observed a 61.7% reduction in the mean error.

I. INTRODUCTION

Common forms of advanced hearing loss are the result of hair cell damage; hearing can be partially restored by means of a cochlear implant. This device incorporates an array of electrodes placed within the cochlea and transmits sound by injecting current into surviving fibers of the auditory nerve. Cochlear implants designed by Cochlear Ltd. contain a stiffening wire (stylet) that straightens the electrode array to assist in the insertion process. In order for the electrode array to curl within the cochlea and avoid damage to the sensorineural epithelium, it is recommended that the “off-stylet” technique is used. The Advance-off Stylet (AoS) technique requires the surgeon to remove the stylet just before the electrode array reaches the basal turn of the cochlea. Although there exist other electrode designs, this paper is primarily concerned with off-stylet implants.

In order to access the cochlea, the surgeon first performs a mastoidectomy and opens the facial recess to expose the cochlea. Once the cochlea is in view, a microdrill is used to open the scala tympani at the base of the cochlea. The surgeon, using a stereomicroscope for guidance, then slowly inserts the cochlear implant electrode array until a standardized mark on the implant is aligned with the cochleostomy site. This mark indicates the position at which the stylet should be stabilized. The surgeon grips the stylet

with forceps and continues to push the electrode array further into the cochlea. Because the electrode array is naturally curved, pushing it off of the stylet causes it to curve into the spiral of the cochlea. The stylet is removed while the surgeon holds the implant array with forceps, and the insertion is then complete [1]. The insertion of the electrode array risks injury to membranous components of the cochlea, even in the hands of highly trained surgeons [2].

There are several limitations with the current practice of cochlear implant insertion, the most significant of which are the lack of visibility which essential blinds the surgeon from the precise point of off-stylet deployment of the array, the sensitivity of the cochlea’s inner structures, and the precision required of the surgeon. The impact of these problems could be lessened by a robot-assisted approach to the procedure.

During insertion of the implant, the surgeon has visualization only of the cochleostomy site. The bony wall of the cochlea prevents direct visualization of the electrode array as it advanced through the cochlear turns. The only source of visible feedback to inform the surgeon of the location of the tip of the implant is the mark on the electrode array that correlates with the depth of insertion and indicates the point at which off-stylet electrode advancement should be initiated. This mark is created by the implant manufacturer and thus fails to account for variance in cochlear anatomy [3]. There is also no good indicator of the implant’s rotation about the axis of insertion.

A challenging requirement in array insertion is minimizing the damage to the basilar membrane, which houses the cochlear sensorineural epithelium. The cochlear sensorineural epithelium may contain residual mechanosensory hair cells, which can allow for preserved detection and processing of auditory information. Damage to the sensorineural epithelium reduces the residual hearing of patients receiving cochlear implantation, which can reduce their hearing outcomes [4] and produce damage to auditory neuronal fibers [5], the targets of electrical stimulation. The small scale of the cochlea in which the implant must be navigated necessitates a high level of precision during the insertion procedure. If the implant is inserted or aligned incorrectly, severe intracochlear damage can result, particularly if the basal turn is not negotiated atraumatically by the tip of the electrode array [6].

Several robot-assisted systems for improving this process have been proposed in the past. Zhang *et al.* designed a system [7] that mounts a “steerable” electrode array, which can be bent in many different shapes, to a robot. The shape of the electrode array during the insertion process is calculated

*Research supported in part by Cochlear Americas, the Sidgmore Family Foundation, and Johns Hopkins internal funds.

P. Wilkening, B. Gonenc, R. H. Taylor, and I. Iordachita are with CISST ERC at Johns Hopkins University, Baltimore MD 21218 USA (email: pwilken3,bgonenc1,rht,iordachita@jhu.edu) (Corresponding author: Paul Wilkening, phone: 973-479-0507; email: pwilken3@jhu.edu).

J. U. Kang is with the Department of Electrical and Computer Engineering at Johns Hopkins University, Baltimore MD 21218 USA (email: jkang@jhu.edu).

W. Chien is with the Department of Otolaryngology at the Johns Hopkins School of Medicine, Baltimore MD 21287 USA (email: wchien1@jhmi.edu).

John Niparko is Chair of Otolaryngology – Head and Neck Surgery at the University of Southern California (email: niparko@med.usc.edu).

to match the curve of the scala tympani, allowing the implant to be inserted without touching the wall of the scala tympani. Another system was proposed by Balachandran *et al.* [8] that assists in percutaneous cochlear implantation. Instead of exposing the temporal bone and drilling a hole to access the cochlea, a hole is drilled straight through the mastoid air cells into the cochleostomy site. Their implant-deploying device is then fitted to a “micro-table” fixture which aims it towards the round window. There is a physical stop for the implant holder when the deployment point is reached, and so once that happens the implant is inserted by continuing to push the electrode array. From the surgeon’s perspective, a plunger must simply be pushed for the entire insertion to be performed. This makes the process simpler, but at the cost of less intraoperative control over the implant’s deployment position. This insertion tool has also been tested with incorporated force sensing [9]. Other work by the same group [10] has involved the implementation of a 3 degrees-of-freedom parallel robot designed specifically for use in cochlear implantation surgery with force sensing capabilities. How closely the force readings during the procedure match force profiles, which have been extensively characterized [11], gives a good indication of how safely the implant was inserted. While prior approaches use novel techniques for improving upon the cochlear implant insertion process, they don’t provide enough control over the placement of the implant’s deployment point.

Virtual fixtures are defined as constraints on the motion of a robot-assisted system, and in medical applications are able to resist movement into areas that would be hazardous to the patient. Virtual fixtures are also able to “pull” the robot into an ideal position. The application of virtual fixtures to robot-assisted surgery has had success in past cooperatively controlled surgical robots (e.g., [12,16]). For cochlear implantations, virtual fixtures can assist in the safe guidance of an implant mounted to a robot to the appropriate deployment point of the implant by ensuring no collisions occur.

In this paper, we present a robot-assisted system for off-stylet cochlear implant insertion. This system, in order to improve upon the reliability of the standard implant insertion process, uses pre- and intra-operative optical coherence tomography (OCT) imaging to set up virtual fixtures based on the patient-specific cochlear anatomy. We then conduct an experiment in which we attempt to reliably reach the ideal deployment point in a cochlear phantom with the tip of an implant using several insertion methods to compare their accuracy and repeatability.

II. METHODS

We use a two-step procedure for robot-assisted cochlear implant insertion: (1) acquire OCT images to construct virtual fixtures, (2) insert the implant into the cochlea under robot guidance based upon the constructed virtual fixtures. The protocol for implantation trials is presented in Fig. 1.

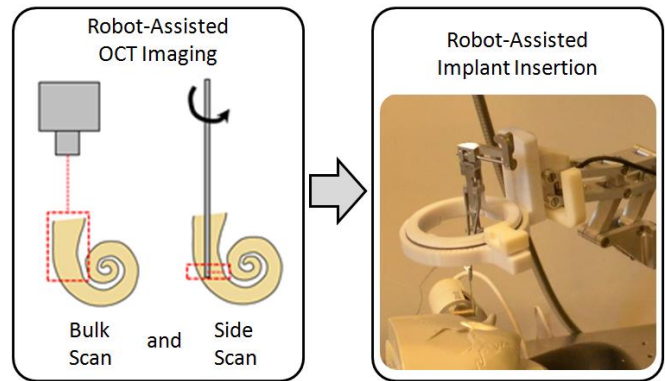


Figure 1. General workflow.

A. OCT Imaging

Two methods of OCT imaging are used in this system: a bulk-volume OCT scanner [13] and a side-viewing OCT probe [14]. Once the bulk scanner is mounted to the robot and positioned to view down the cochlear channel, it can take $5 \times 5 \times 5 \text{ mm}^3$ OCT volume image of the cochlear interior per scan. Multiple scans at different axial and transverse positions and stitching them allows imaging and registration of the cochlear (scala tympani) lumen. The volume shows the initial curvature of the basal turn relative to the cochleostomy site unambiguously, which is an important landmark when determining the ideal deployment position. However, the sides of the cochlear interior are often not visible due to the limited viewing angle [9].

The side-viewing probe is an optical fiber contained within a steel tube. A window is cut into the side of the tube near the end of the fiber, through which the fiber emits and receives light. When rotated by a motor and inserted into the cochlea, it captures contours of the interior wall of the cochlea at its current depth. While this method is able to give high resolution imaging of the walls of the cochlear interior, it doesn’t capture the entrance to the cochlea or basal turn. In order to fill in the gaps of information from each imaging method, these scans are registered to the bulk volume and a new model is created.

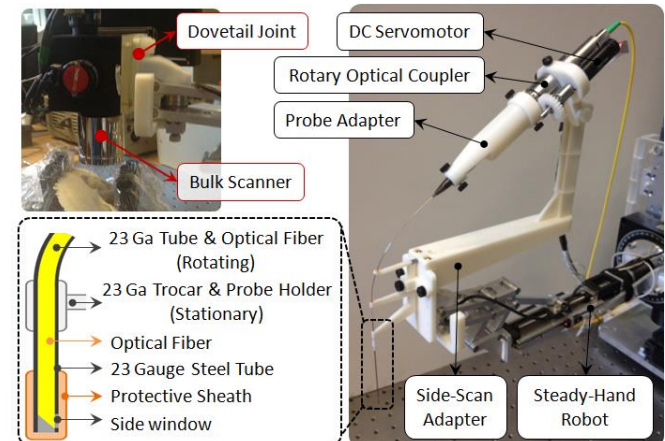


Figure 2. Imaging adapters for the bulk scanner and the side-viewing probe. The adapters mount on the robot arm with high repeatability and ensure coaxial imaging axes.

B. Steady-Hand Robot for Cochlear Implant Insertion

The steady-hand robot [15] is a cooperatively controlled device where the surgical tool is held simultaneously by the operator and an actively controlled robot arm. The robot utilizes XYZ linear stages for translation, a rotary stage for rolling, a tilting mechanism, and a tool adaptor with a force sensor. The robot senses forces exerted by the surgeon on the tool and moves to comply, thus providing intuitive control of tremor-free, precise motion.

We have developed removable adapters for attaching our bulk-scan and side-scan OCT imagers to the robot (Fig. 2). These adapters are attached on the robot arm through a dovetail joint so that they are easily replaced with high repeatability (0.5 mm at the implant tip for our 3D printed prototype, but potentially much higher for a machined version). The same dovetail is used for attaching the implant insertion tool so that the imaging central axis coincides with the axis of the insertion tool. After calibration, this ensures that the OCT coordinate system used to guide the insertion is registered to the robot coordinate system.

The bulk scanner adapter is a simple fixture for the robot arm to hold the scanner. The side-scan adapter holds a DC servomotor and a rotary optical coupler to spin the imaging probe at a constant speed. In order to provide a clear line of sight through the microscope, the motor and the optical coupler are held away from the insertion site by using a longer imaging probe, and bending it at a slight angle. The imaging probe is guided through two 23 gauge trocars to minimize wobble while spinning.

The implant insertion adapter is shown in Fig. 3. The implant holding device is attached to a 65 mm inside diameter circular slim ball bearing in order to permit the axial rotation of the implant to be adjusted while still providing a clear line of sight from the microscope to the cochlear opening. The bearing can be locked by pushing a knob on the handle to fix the axial orientation. Attached to the inner ring of the bearing are graspers holding the implant electrode array at two points. The graspers are spring-loaded with a tendency to close. They can be opened by rotating a cam on the handle in order to attach or remove the electrode array.

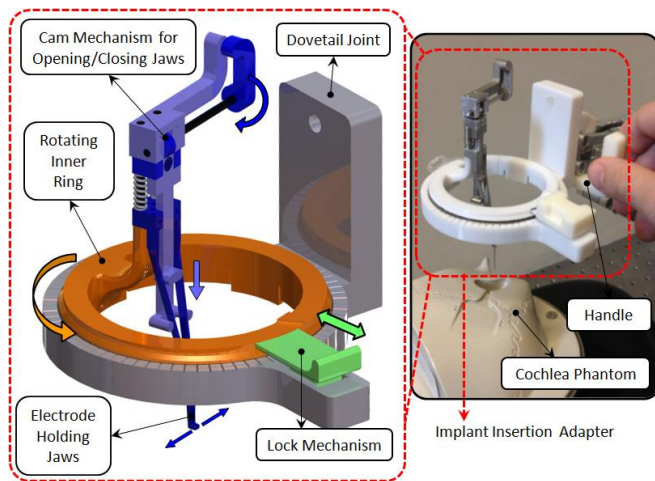


Figure 3. Implant insertion adapter. It slides on the robot arm via the dovetail joint and ensures the insertion and imaging axes to be coaxial.

During the procedure, the cam is rotated to open the graspers, and then the straight electrode is attached on the spring-loaded tool. The axial rotation of the electrode is corrected and the bearing is locked. The surgeon grasps a handle on the tool holder (Fig. 3) and guides the robot to insert the implant until the first basal turn. The graspers are reopened by rotating the cam. The electrode is taken out, and the cam is released to squeeze only the stylet between the graspers. The electrode is held using tweezers and advanced into the cochlear canal until the ribs on the implant reach the cochleostomy site, which completes the insertion.

C. System Integration and Workflow

Fig. 4 outlines the interactions between our system components. The first step in our proposed workflow is to acquire OCT images of the cochlear interior through the use of either the bulk scanner or the scanning sideview probe. Bulk scan volumetric images are obtained simply by mounting the scan head on the robot and using cooperative “steady-hand” guiding to position it to look down the cochlea while observing the scanned images on a display monitor.

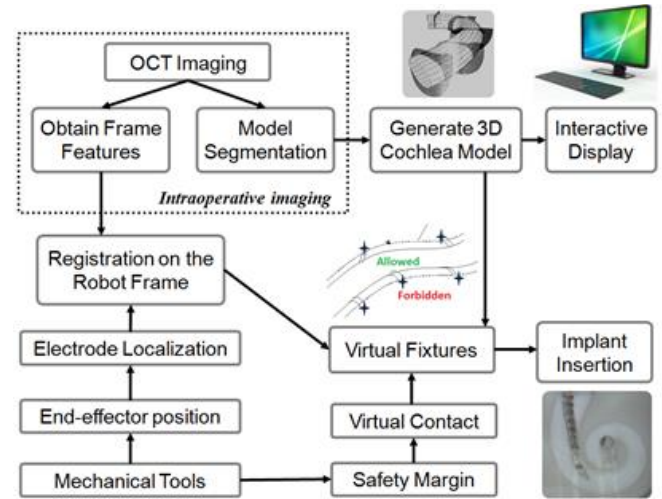


Figure 4. Detailed workflow and interaction between system components.

The sideview probe, however, requires insertion into the cochlea in order to obtain images and needs an adaptive virtual fixture to ensure that it doesn’t collide with the basilar membrane during its insertion. A model of the interior of the cochlea is built up from a succession of cross-sectional contours created from 360° OCT scans taken as the probe is guided into the cochlea. The center of each cross-section is determined, and a virtual fixture is created to minimize the sum-of-squares distance from these center points and the tool shaft of the probe, using the basic optimization framework discussed in [12,16]. At each time-step of the robot’s control loop, the optimization framework determines the incremental joint values Δq of the steady hand robot that minimizes the expression:

$$w_F \| [\boldsymbol{\varepsilon}, \boldsymbol{\alpha}]^T - K\mathbf{f} \|^2 + w_{VF} \sum_i \| \mathbf{t} + \boldsymbol{\alpha} x \mathbf{t} + \boldsymbol{\varepsilon} - (\mathbf{c}_i - \mathbf{p}_i) \|^2$$

such that $[\boldsymbol{\varepsilon}, \boldsymbol{\alpha}]^T = J(\mathbf{q})\Delta\mathbf{q}$

This calculates the incremental joint values based on a weighted combination of force compliance, which moves the robot according to forces observed at its handle, and the sideview virtual fixture, which pulls the probe in the

direction of the cochlea's central axis. Here, ϵ and α represent the incremental translational and rotational movements of the robot, respectively. w_F is a scalar that corresponds to the relative weight of the force compliance, and w_{VF} corresponds to the relative weight of the sideview virtual fixture. K is a matrix of gains for the force sensor, and f is a vector of force and torque values read from the force sensor. As illustrated in Fig. 5, t is the position of the probe tip, c_i is the position of the i -th center point read by the sideview probe, and p_i is the projection of the i -th center point onto the probe's axis. $J(q)$ is the jacobian that transforms the robot's joint space into Cartesian space, and Δq is a vector of incremental joint movements. Note that the second term is a sum over all center points read by the sideview probe.

The guiding process stops when the contours begin to "open up" in the direction of the cochlear turn. The penetration depth is remembered as the stopping point for implant insertion, and the probe is withdrawn using a virtual fixture to constrain motion along its axis.

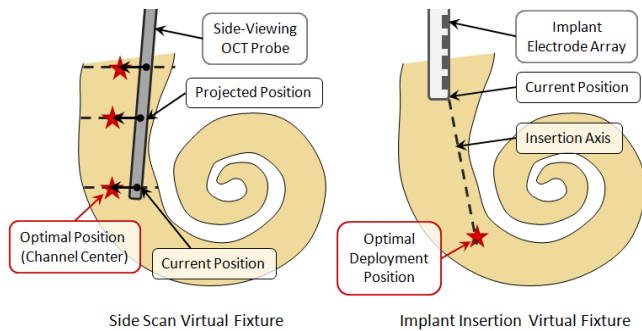


Figure 5. Virtual fixtures for the side scan (left), in which the side scan probe is guided towards the central axis of the cochlear channel to prevent collision with the side walls, and for implant insertion (right), in which the implant is guided towards the optimal deployment point and further advance is inhibited.

The next step is to insert the electrode array. The implant is attached to the insertion adapter, which is mounted to the robot. The surgeon guides the implant to the cochlear entrance using force compliance, and enacts a virtual fixture for implant insertions. This virtual fixture uses an ideal deployment point that is either based on OCT imaging, for our clinical workflow, or a prior insertion, for implant insertion experiments. As the surgeon advances the implant, motion is constrained so that the tip of the implant is guided along the axis between its current position and the optimal point as shown in Fig. 5. When the implant reaches the desired target position, advancing further is inhibited, so the deployment from the stylet can be performed.

III. EXPERIMENT

In the proposed procedure, the accuracy of implant placement depends on three factors: 1) the accuracy of the imaging and cochlear model construction; 2) accurate registration of the robot to this model; and 3) accurate guidance of the implant along the desired axis to the desired target deployment point determined by the model. Here we report preliminary experiments to compare the accuracy of implant placement at the target using conventional freehand methods to robot-assisted methods, once the desired

placement path has been determined. We also assess the effect of adding an insertion-guiding virtual fixture based purely on a saved goal position to force-compliant steady-hand guidance.

A. Setup

A cochlear phantom and robot are positioned so that the surgeon/user can guide the implant insertion tool into the cochlear canal while observing the procedure using a standard surgical microscope, as shown in Fig. 6. We use a standard cochlear insertion training phantom provided by Cochlear Americas. This phantom has a cutaway providing a window permitting a video camera to observe the implant as it is inserted into the cochlear canal. Video is captured during each insertion trial and saved for offline processing, but the surgeon is not able to observe the video during insertions.

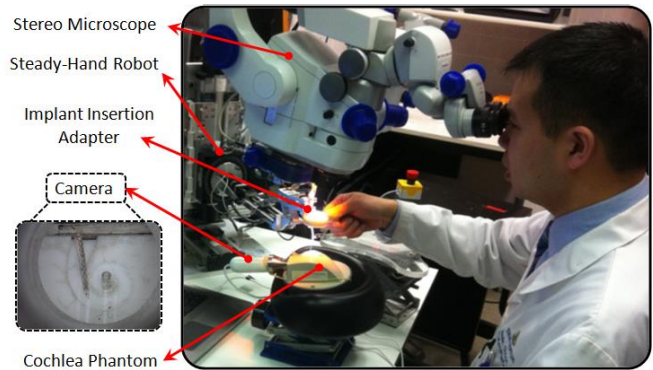


Figure 6. Setup for implant insertion repeatability experiments on an artificial cochlea phantom. The clinician uses the microscope for guidance. The camera inserted into the phantom is used for assessment after the trial.

For this experiment, a Cochlear Nucleus 24 Contour Advance Practice Electrode implant (Cochlear Americas, Centennial, CO) was modified by replacing its stylet with a 33 Ga steel tube. This tube is stiffer than a stylet that would be used clinically in order to facilitate reuse of the same implant for multiple insertion experiments. The standard stylet is designed for single-use, and we observed that the implant shape tended to get bent unpredictably over multiple insertions. Even with manual re-straightening, it proved essentially impossible to restore the implant shape to its out-of-the-box condition for each insertion trial. Fig. 7 shows the condition of an implant with the original stylet at the start of insertion trials and after ten trials and manual re-straightening.



Figure 7. Cochlear implant with original stylet before ever being used (right) and after ten insertion trials and manual re-straightening (left). Note the significant shape change.

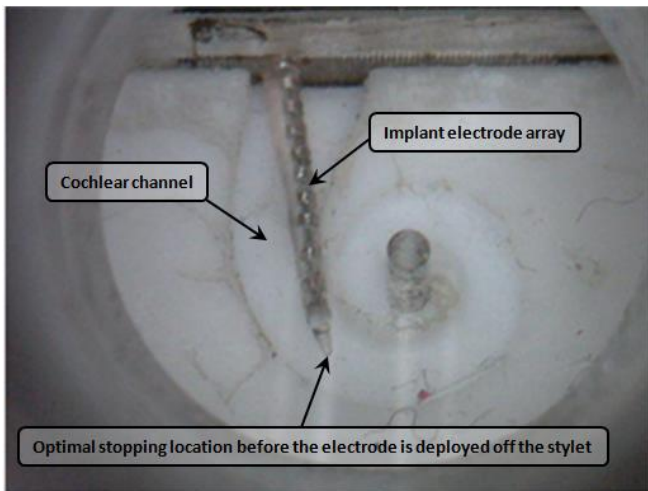


Figure 8. Cochlear phantom interior with implant inserted to an ideal deployment position. This view is given by the internal camera.

To determine the ideal insertion position, one of our otolaryngologist co-authors (Dr. Chien) inserted the implant while observing the implant position on a monitor showing the view seen by the using the phantom’s built-in camera. This ideal deployment point, determined by the surgeon based on his clinical experience, was saved to construct the insertion virtual fixture and assess insertion accuracy. This position can be seen in Fig. 8. During insertion experiments, video from the phantom’s built-in camera was captured and saved but was hidden from the surgeon/user.

B. Procedure

Our experiment consisted of three consecutive sets of five implant insertions. The first set of insertions had the implant mounted to the robot, and used the virtual fixture based on the saved frame as a guide. The second set of trials also had the implant mounted to the robot, but the robot itself was only used for tremor reduction, not virtual fixtures. Here, the surgeon used the depth mark on the implant to determine when the ideal deployment position was reached. For the final set of insertions, the surgeon inserted using the standard manual procedure. These insertions were performed identically to a typical cochlear implant surgery. To avoid possible repeatability error due to the dovetail joint, the implant isn’t dismantled between saving the ideal deployment point during the setup and the implant insertion trials. After the surgeon’s insertions were complete, the entire process was repeated with a novice graduate student co-author as the user. During each of these trials, we recorded the end position of the electrode array. To negate the effects of a learning curve, a brief training period was allowed for the surgeon to adjust to each of the various methods of insertion before data was recorded.

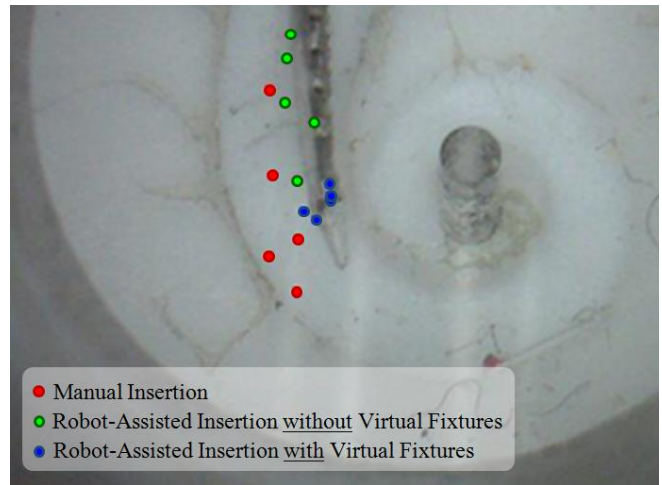


Figure 9. Endpoints of the electrode array for all three insertion types with the novice as the user.

IV. RESULTS

Table I and Fig. 11 show an assessment of the accuracy of the insertions, or how close the surgeon and novice were able to get the implant tip to the desired deployment point. When compared to his manual insertions, the surgeon’s mean error for both sets of robot-based implantations decreases by about 0.7 mm. For the novice user, enacting the virtual fixture lowers the error by about 1.4 mm.

TABLE I. IMPLANT PLACEMENT ACCURACY RESULTS

User	Insertion Type	Mean*	Std. Dev.*	Max.*	Min.*
Surgeon	Manual	1.33	0.16	1.51	1.14
	Robot-Assisted (without VF)	0.62	0.29	0.83	0.13
	Robot-Assisted (with VF)	0.51	0.17	0.69	0.3
Novice	Manual	1.67	0.62	2.57	0.97
	Robot-Assisted (without VF)	2.22	1.10	3.48	0.75
	Robot-Assisted (with VF)	0.3	0.19	0.52	0.08

* Values correspond to the distances between the implant endpoints and the ideal deployment point. Units are in mms.

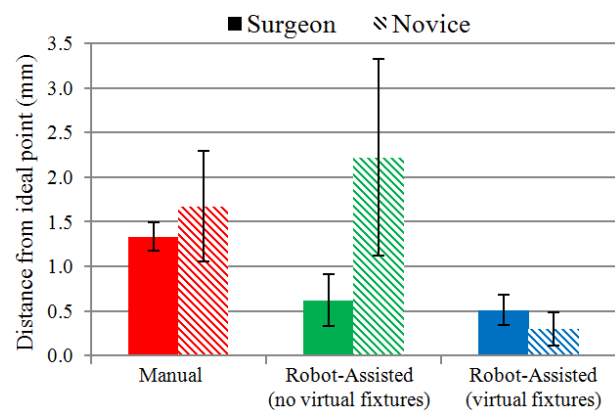


Figure 10. Implant placement accuracy chart. Each bar corresponds to the mean distance for its trial, while the lines extending above and below show the standard deviation.

Table II and Fig. 12 summarize the repeatability of the experiment, or how consistently the user is able to insert the implant to the same point, regardless of how close that point is to the target. The numbers reported are the mean and standard deviation of the distances of insertions from the mean insertion points for each experimental condition. The surgeon's mean implant repeatability was about 0.1 mm greater with robot-based insertion methods than that for manual placement. The novice user's mean repeatability errors decreased from 1.3 mm with the manual method to 0.94 mm with the robot-assisted method without virtual fixtures and to 0.31 mm with virtual fixtures.

TABLE II. IMPLANT PLACEMENT REPEATABILITY RESULTS

User	Insertion Type	Mean*	Std. Dev.*	Max.*	Min.*
Surgeon	Manual	0.15	0.06	0.24	0.09
	Robot-Assisted (without VF)	0.24	0.19	0.56	0.04
	Robot-Assisted (with VF)	0.25	0.15	0.51	0.17
Novice	Manual	1.30	0.77	2.48	0.68
	Robot-Assisted (without VF)	0.94	0.57	1.66	0.20
	Robot-Assisted (with VF)	0.31	0.10	0.41	0.19

* Values correspond to the distances between the implant endpoints and the centroid for their insertion type. Units are in mms.

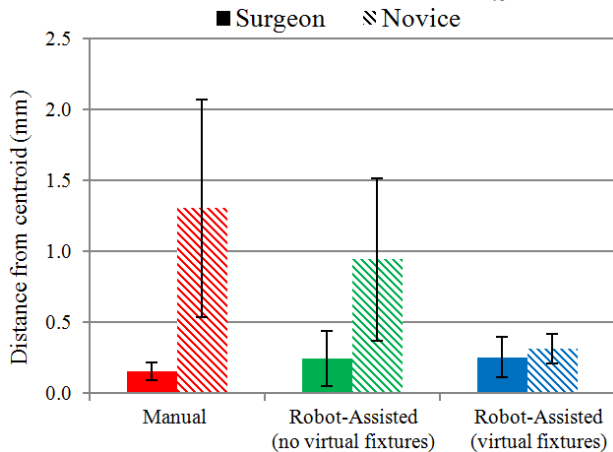


Figure 11. Implant placement repeatability chart. Each bar corresponds to the mean distance for its trial, while the lines extending above and below show the standard deviation.

V. DISCUSSION

Fig. 11 shows that the robot-assisted insertions with virtual fixtures have the highest mean accuracy for both the surgeon and novice users. This chart demonstrates that even a novice is able to achieve approximately 1 mm greater accuracy utilizing this system than the current standard procedure produces with an experienced surgeon. We performed an ANOVA (analysis of variance) test on our results, showing that there was a statistically significant difference between the mean values for the insertion types of each user ($p < 0.05$) except for the surgeon's precision results ($p = 0.4973$). ANOVA can only show that at least one of the mean values is significantly different the others for each set of trials, so the next step is to determine which mean values are different to a level of significance. We used Welch's t-test, because of the presence of unequal variances

in our ANOVA results, to calculate the p-values of directly comparing the insertion types of each user (Table III). In statistical significance testing, the p-value is the probability of obtaining a test statistic at least as extreme as the one that was actually observed. Both robot-based methods were shown to be significantly more accurate than the standard practice for the surgeon ($p = 0.0014$ without virtual fixtures, $p = 0.00002$ with virtual fixtures), and for the novice the virtual fixture shows a statistically significant accuracy improvement over both of the other insertion methods ($p = 0.0027$ compared to manual, $p = 0.0092$ compared to robot-assisted) (Table III).

TABLE III. P-VALUES FOR THE INSERTION TRIALS

User	Insertion Type**	Accuracy			Repeatability		
		M	R	V	M	R	V
Surgeon	M	-	0.0014*	0.00002*	-	0.1813	0.1060
	R	0.0014*	-	0.2446	0.1813	-	0.4660
	V	0.00002*	0.2446	-	0.1060	0.4660	-
Novice	M	-	0.1843	0.0027*	-	0.2115	0.0234*
	R	0.1843	-	0.0092*	0.2115	-	0.0378*
	V	0.0027*	0.0092*	-	0.0234*	0.0378*	-

* Results with high statistical significance.

** Insertion type M refers to the manual trials, insertion type R refers to robot-assisted trials without virtual fixtures, and insertion type V refers to robot-assisted trials with virtual fixtures.

The difference between the accuracy of robot assistance with and without virtual fixtures, however, was not statistically significant for the surgeon ($p = 0.2446$) (Table III). On the day of the experiment, the surgeon was provided with ample light and a clear line of sight to the indicating mark on the implant array, as well as a well-defined reference at the entrance to the phantom cochlea. In reality, the visibility might be more limited within a patient's temporal bone. The virtual fixture's imaginary barrier should function as well in both scenarios, and so this approach could better represent the heightened accuracy of employing the virtual fixture. We plan to conduct further experiments that include trials using the adaptive virtual fixture with a higher number of repetitions better simulating the conditions of the OR in order to more accurately determine the extent to which the virtual fixtures make a difference.

The virtual fixture-based method produced statistically better repeatability for the novice than the other insertions ($p = 0.0234$ for freehand and $p = 0.0378$ for no virtual fixtures) (Table III), but the surgeon's robot-based insertions resulted in slightly less consistent placement than his manual insertions. For the novice, manual insertions have low precision because of the low visibility involved in that process, and our virtual fixture-based insertions increase the repeatability of these trials significantly by guiding the novice back to a predetermined point. The surgeon's placement variability results were mildly surprising to us, since similar experiments for other surgical tasks have generally shown more consistency for robot-assisted manipulation, especially if virtual fixtures are present. Indeed, this is what we observed with our novice user.

However the observed difference of 0.1 mm for the surgeon was not statistically significant ($p = 0.1813$ and $p = 0.106$). Fig. 9 shows that one of the surgeon's placements using the virtual fixtures was an outlier, significantly reducing the corresponding repeatability results. This may be due to a deformation of the implant's shape, but a more extensive study is necessary. It is also possible that the results are due to the experience of the surgeon with manual implantations, enabling him to more reliably repeat the specific hand movements used for these insertions, although the low visibility still decreases the placement accuracy with manual insertions. By having the surgeon spend more time practicing insertions using the robot's force sensors for guidance, the placement repeatability for trials that use the robot may exceed that of the manual practice, as seen with the novice user.

VI. CONCLUSION

The precision of the initial array placement to a cochlear depth that would enable effective negotiation of the first cochlear turn is advanced by a robot-assisted implant insertion technique based on virtual fixtures. The system described offers an effective strategy for managing variance in cochlear morphology and averting damage to soft tissues within the cochlea.

The enhanced accuracy and precision of the novice when using the virtual fixture indicate that this system may work well for teaching inexperienced surgeons to perform an implantation. The act of the implant being safely guided to an ideal deployment point with a simple advancement can illustrate to a student the proper insertion angle and depth necessary to perform a manual insertion without guidance.

Future work with this system will involve the assessment of the accuracy and repeatability of implant insertions that use virtual fixtures constructed with OCT imaging. The errors involved in the imaging process and in registering the constructed model to the robot will be measured, as well as the implant placement error. More insertions will be conducted with additional users to reduce the possibility of a learning curve, and a full insertion will be performed by the surgeon into a cadaveric temporal bone. Using virtual fixtures based on OCT imaging to insert an implant into a human cochlea will better assess the full clinical approach to cochlear implantation outlined in this paper.

ACKNOWLEDGMENT

Partial support for this project was provided by Cochlear Americas and the Sidgmore Family Foundation. The authors thank Emily Daggett for her contributions towards the software infrastructure.

REFERENCES

- [1] Cosetti, M., and Roland Jr, J. T. Cochlear implant electrode insertion. *Operative Techniques in Otolaryngology, head & neck surgery* 21, 4 (Dec. 2010), 223-232.
- [2] O. Adunka, et al. "Preservation of basal inner ear structures in cochlear implantation." *ORL* 66.6 (2005): 306-312.
- [3] T. R. McRackan, et al. "Comparison of Cochlear Implant Relevant Anatomy in Children Versus Adults." *Otology & Neurotology* 33.3 (2012): 328.

- [4] R. F. Brown, et al. "Residual hearing preservation after pediatric cochlear implantation." *Otology & neurotology: official publication of the American Otological Society, American Neurotology Society [and] European Academy of Otology and Neurotology* 31.8 (2010): 1221.
- [5] P. A. Leake-Jones and S. J. Rebscher, "Cochlear pathology with chronically implanted scala tympani electrodes." *Annals of the New York Academy of Sciences* 405 (1983): 203-223.
- [6] D. W. Kennedy. "Multichannel intracochlear electrodes: Mechanism of insertion trauma." *The Laryngoscope*, vol. 97, pp. 42-49. 1987
- [7] J. Zhang, et al. "Inroads toward robot-assisted cochlear implant surgery using steerable electrode arrays." *Otology & Neurotology* 31.8 (2010): 1199-1206.
- [8] R. Balachandran, et al. "Insertion of electrode array using percutaneous cochlear implantation technique: a cadaveric study." *Proc. SPIE*. 7964 (2011).
- [9] D. Schurzig, R. F. Labadie, A. Hussong, T. S. Rau, and R. J. Webster, "Design of a Tool Integrating Force Sensing With Automated Insertion in Cochlear Implantation", *Mechatronics, IEEE/ASME Transactions on*, 17- 2 (2012): 381-389.
- [10] Pile, J. and Simaan, N. Modeling, Design, and Evaluation of a Parallel Robot for Cochlear Implant Surgery. *IEEE/ASME Transactions on Mechatronics* (March,2014) 1-10.
- [11] Miroir, M., Nguyen, Y., Kazmitcheff, G., Ferrary, E., Sterkers, O., and Grayeli, A. B. Friction force measurement during cochlear implant insertion: application to a force-controlled insertion tool design. *Otology & neurotology : official publication of the American Otological Society, American Neurotology Society [and] European Academy of Otology and Neurotology* 33, 6 (Aug. 2012), 1092-100.
- [12] J. Funda, R. Taylor, B. Eldridge, S. Gomory, and K. Gruben, "Constrained Cartesian motion control for teleoperated surgical robots", *IEEE Transactions on Robotics and Automation*, 12- 3 (1996): 453-466.
- [13] M. Zhao, et al. "Sensing and three-dimensional imaging of cochlea and surrounding temporal bone using swept source high-speed optical coherence tomography." *SPIE BiOS*. International Society for Optics and Photonics, 2013.
- [14] S. Gurbani, M. Zhao, P. Wilkening, B. Gonenc, G. Cheon, I. Iordachita, W. Chien, R. Taylor, J. Niparko, J. Kang. "Swept Source Optical Coherence Tomography Imaging of Temporal Bone for Use in a Robot Assisted Surgical Guidance System for Cochlear Implant Surgery," presented at the Biomedical Optics Express Conference, Seattle, Washington, 2013.
- [15] X. He, et al. "Toward clinically applicable Steady-Hand Eye Robot for vitreoretinal surgery." *ASME 2012 International Mechanical Engineering Congress and Exposition*. American Society of Mechanical Engineers, 2012.
- [16] A. Kapoor, M. Li, and R. H. Taylor "Constrained Control for Surgical Assistant Robots." *IEEE Int. Conference on Robotics and Automation*, Orlando, May 15-19, 2006, pp. 231-236.